Optical coupling method utilizing a lensed fiber integrated with a long-period fiber grating

Wen Tzung Chen and Lon A. Wang

A novel optical coupling scheme that uses a lensed fiber integrated with a long-period fiber grating (LPFG) is proposed. Two experiments are performed to demonstrate the validity of such a scheme in single-mode-fiber–single-mode-fiber (SMF-to-SMF) and laser-diode–single-mode-fiber (LD-to-SMF) coupling setups. The measured results show that for an appropriate lens radius the addition of a LPFG will lead to a higher coupling efficiency over a longer range of working distance than without the LPFG. Coupling efficiencies of ~78% and 35% are achieved for corresponding working distances of ~250 and 110 μm, 1-dB longitudinal tolerances of ~40 and 26 μm, and 1-dB transverse tolerances of ~7.6 and 2.6 μm for SMF-to-SMF and LD-to-SMF, respectively. © 2000 Optical Society of America

OCIS codes: 060.2310, 050.2770.

1. Introduction

Recently, long-period fiber gratings (LPFG's) have been used in various applications such as band-rejection filters, gain equalizers, rocking filters, mode converters, and sensors.[1–5] Here we propose a new application in which a LPFG and an integrated hemispherical lensed fiber are used to assist optical coupling.

Various schemes that use lensed fibers have been reported in the past few years for applications of single-mode-fiber–single-mode fiber (SMF-to-SMF) and laser-diode–single-mode-fiber (LD-to-SMF) coupling.[6–9] Practically, a lensed fiber has many desirable features, such as high coupling efficiency, compactness, mechanical stability, and economical performance. However, a lensed fiber also has several disadvantages, such as a small working distance (roughly shorter than its core diameter, ~10 μm), tight transverse tolerance (~0.3 μm for 1-dB loss), and critical constraints on the fabrication process (lens radius, ≅5 μm). A working distance longer than ~100 μm is generally desired for LD-to-SMF packaging of an optical subassembly module[10] and for the reduction of optical backreflection. For example, in the case of lensed fiber with a 50-μm radius, the optical backreflection decreases from −30 to −60 dB when the working distance increases from 10 to 100 μm.[11] Although it has been reported that an integrated spot size converter improves coupling,[12] the working distance is typically not more than 20 μm; thus higher optical backreflections can be induced for an uncoated and cleaved fiber. Various approaches to increasing the working distance have been tried, but most working distances are still limited to less than 50 μm.[13,14] Although the use of thermally expanded core fiber integrated with a coreless fiber could lead to a larger working distance, the fabrication processes with this type of fiber are relatively time consuming and complicated.[10] For example, the fabrication of a thermally expanded fiber may require 1 h at 1700 °C, and three different fibers may be needed for integration.

To overcome these disadvantages, we propose the novel coupling scheme shown schematically in Fig. 1, in which ray optics is used for qualitative analysis. In Section 2 we present a more rigorous analysis. A portion of the rays coming from a finite source is coupled into the cladding of a receiving single-mode fiber, SMF1, by a hemispherical lensed fiber. These rays pass through the LPFG in region III and diffract into different orders. The diffracted rays that satisfy the total internal reflection condition

$$\theta_4 = \sin^{-1}\left\{\frac{1}{n_{co}}\left[n_{cl}\sin\theta_3 + m\left(\frac{\lambda}{\Lambda}\right)\right]\right\} > \sin^{-1}\left(\frac{n_{cl}}{n_{co}}\right) \quad (1)$$

The authors are with the Department of Electrical Engineering and Institute of Electro-Optical Engineering, National Taiwan University, Taipei, Taiwan. L. A. Wang's e-mail address is lon@ccms.ntu.edu.tw.

Received 14 January 2000.
0003-6935/00/254490-11$15.00/0

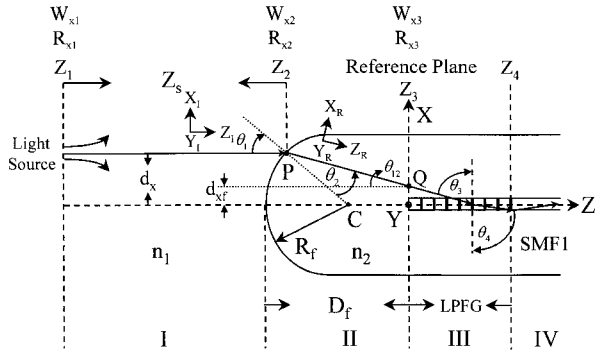

Fig. 1. Schematic diagram of the proposed novel optical coupling scheme. Abbreviations are defined throughout the text.

remain propagating in the core. Here θ_3 and θ_4 are the incident and diffraction angles, respectively; m is an integer, Λ is the period of the LPFG; and n_{co} and n_{cl} are the refractive indices in the core and the cladding, respectively. The other rays received by the core of SMF1 are coupled into the cladding because of the presence of the LPFG.

As we reported previously,[15] the main advantage of using such a coupling scheme is the resultant long working distance because the launched beam is coupled to the relatively large cladding area relative to the core area. Although the LPFG plays a vital role in assisting coupling, fabrication of the LPFG is simple.[16–19] The radius of the lensed fiber used in this coupling scheme is larger than that of a conventional fiber, which permits the fabrication tolerances to be relaxed. Therefore the proposed lensed fiber assisted by a LPFG may serve as a useful coupling device in the packaging of an optical subassembly.

The remainder of this paper is arranged as follows: In Section 2 we use a mode-expansion method, including core and cladding modes, to calculate the coupling efficiency. In Section 3 two we demonstrate proofs of experiment to show the validity of the proposed scheme. In Section 4 we first discuss the differences between the measured and simulated results and then analyze the optimal working distance and lens radius for the proposed scheme. Moreover, we discuss some practical applications of the scheme. Finally, we conclude our study in Section 5.

2. Principle

First we use an *ABCD* matrix to locate a Gaussian beam and then we apply the mode-expansion method to calculate the coupling efficiency of a Gaussian beam and a fiber cladding mode. As shown in Fig. 1, a Gaussian beam initially located at plane Z_1 has a beam waist $W_{x1} = W_0$, a radius of curvature $R_{x1} = \infty$, and a transverse displacement d_x. After the beam has propagated a distance Z_s in free space, the new waist W_{x2} and radius of curvature R_{x2} at plane Z_2 can be expressed as

$$W_{x2} = W_0\left[1 + \left(\frac{Z_s}{Z_0}\right)^2\right]^{1/2}, \tag{2}$$

$$R_{x2} = Z_s\left[1 + \left(\frac{Z_0}{Z_s}\right)^2\right], \tag{3}$$

where $Z_0 = n_1\pi W_0^2/\lambda_0$, and n_1 is the refractive index of region I.

The Gaussian beam is incident upon the lensed fiber at an angle θ_1 owing to a transverse offset. To match the boundary conditions of the complex phases for the incident and refracted beams at point P we have

$$\phi_1(x_1, y_1, z_1) = \phi_R(x_R, y_R, z_R), \tag{4}$$

where

$$\phi_i(x_i, y_i, z_i) = k_i z_i + \frac{k_i}{2}\left(\frac{x_i}{q_{xi}} + \frac{y_i}{q_{yi}}\right), \tag{5a}$$

$$\frac{1}{q_i} = \frac{1}{R_i} - j\frac{\lambda_0}{n_i\pi W_i^2}, \qquad k_i = 2\pi n_i/\lambda_0, \tag{5b}$$

$i = I, R$ correspond to incident and refracted beams, respectively, and $n_I = n_1$, $n_R = n_2$.

After some derivation, the *ABCD* matrix for the tangential and sagittal planes at location Z_3, denoted M_x and M_y, respectively, can be written as[20,21]

$$M_x = \begin{bmatrix} \left(\frac{\cos\theta_2}{\cos\theta_1}\right) + L_f\left(\frac{n_1\cos\theta_1 - n_2\cos\theta_2}{n_2 R_f\cos\theta_1\cos\theta_2}\right) & L_f\left(\frac{n_1\cos\theta_1}{n_2\cos\theta_2}\right) \\ \frac{n_1\cos\theta_1 - n_2\cos\theta_2}{n_2 R_f\cos\theta_1\cos\theta_2} & \left(\frac{n_1\cos\theta_1}{n_2\cos\theta_2}\right) \end{bmatrix} = \begin{bmatrix} A_x & B_x \\ C_x & D_x \end{bmatrix}, \tag{6}$$

$$M_y = \begin{bmatrix} 1 + L_f\left(\frac{n_1\cos\theta_1 - n_2\cos\theta_2}{n_2 R_f}\right) & L_f\left(\frac{n_1}{n_2}\right) \\ \frac{n_1\cos\theta_1 - n_2\cos\theta_2}{n_2 R_f} & \left(\frac{n_1}{n_2}\right) \end{bmatrix} = \begin{bmatrix} A_y & B_y \\ C_y & D_y \end{bmatrix}, \tag{7}$$

where n_1 and n_2 are the refractive indices in the air and fiber and θ_1 and θ_2 denote the incident and refractive angles, respectively. We assume that $n_{co} \cong n_{cl} = n_2$; other parameters are defined as

$$\theta_1 = \sin^{-1}(d_x/R_f), \tag{8}$$

$$L_f = \overline{PQ} = \frac{D_f - R_f(1 - \cos\theta_1)}{\cos\theta_{12}}. \tag{9}$$

The new waist and radius of curvature for the tangential plane Z_3 can be expressed as

$$W_{x3} = W_{x2}\left[\left(A_x + \frac{B_x}{R_{x2}}\right)^2 + \left(\frac{\lambda_1 B_x}{\pi {W_{x2}}^2}\right)^2\right]^{1/2}, \quad (10)$$

$$R_{x3} = \frac{\left(A_x + \frac{B_x}{R_{x2}}\right)^2 + \left(\frac{\lambda_1 B_x}{\pi {W_{x2}}^2}\right)^2}{\left(A_x + \frac{B_x}{R_{x2}}\right)\left(C_x + \frac{D_x}{R_{x2}}\right) + B_x D_x\left(\frac{\lambda_1}{\pi {W_{x2}}^2}\right)^2}. \quad (11)$$

Similarly, we can obtain the waist and the radius of curvature for sagittal plane Z_3 by replacing subscript x with y. Here we assume Gaussian beam propagation between planes Z_2 and Z_3.

For the small-angle approximation, the normalized electric field E^s of the transformed Gaussian beam expressed in terms of the XYZ coordinates in plane Z_3 is[22]

$$E^s = \left(\frac{1}{\pi}\right)^{1/2}\left(\frac{1}{W_{x3}W_{y3}}\right)^{1/2}\exp\left\{-\left(\frac{(X-d_{xf})^2}{{W_{x3}}^2} + \frac{Y^2}{{W_{y3}}^2}\right) - jk_3\left[\frac{(X-d_{xf})^2}{2R_{x3}} + \frac{Y^2}{2R_{y3}} + \theta_{12}(X-d_{xf})\right]\right\}, \quad (12)$$

where $d_{xf} = d_x - L_f \sin\theta_{12}$ and $k_3 = 2\pi n_2/\lambda_0$.

By using the coordinate transformation and assuming that the polarization of the Gaussian beam is in the Y direction, we can express the exact radial and azimuthal vector components of the electric field as[23,24]

$$E^s(r, \phi) = -jE^s \exp(j\phi)\hat{r} + E^s \exp(j\phi)\hat{\phi}. \quad (13)$$

Depending on the radius of the lens, various amounts of the transformed beam will excite the cladding modes, which are then coupled back into the core mode in region III with the aid of a LPFG. Only the excited cladding modes that are phase matched with the grating can be converted efficiently into the core mode at a specific wavelength. Conversely, a part of the transformed beam that excites the core mode will be coupled out into the cladding when it is phase matched. To calculate the coupling efficiency between the transformed Gaussian beam and each fiber mode, we expand the Gaussian beam as

$$\mathbf{E}^s = \sum_i a_i {E_i}^{\mathrm{co}} + \sum_v b_v {\mathbf{E}_v}^{\mathrm{cl}}, \quad (14)$$

where the superscripts co and cl denote the core and the cladding modes of a fiber, respectively, and subscripts i and v indicate the kinds of mode. The electric field distribution of each cladding mode can be found in the literature.[23] The effect of the radiation modes is negligible because of the modes' relatively small values. Core and cladding modes form a complete orthogonal set, and a_i and b_v are the corresponding coefficients.

The coupling efficiency between the transformed Gaussian beam and the vth cladding mode is defined as

$${\eta_v}^{s-\mathrm{cl}} = \frac{\text{power carried by the } v\text{th excited cladding mode}}{\text{power carried by the Gaussian beam}} = \frac{\frac{1}{2}\mathrm{Re}\left[|b_v|^2 \iint ({\mathbf{E}_v}^{\mathrm{cl}} \times {\mathbf{H}_v}^{\mathrm{cl}^*})\hat{z}\,\mathrm{d}A\right]}{\frac{1}{2}\mathrm{Re}\left[\iint (\mathbf{E}^s \times \mathbf{H}^{s^*})\hat{z}\,\mathrm{d}A\right]}. \quad (15)$$

Similarly, one can obtain the coupling efficiency between the transformed Gaussian beam and the core mode by replacing the superscript cl with co and b_v with a_i.

If the Z component of the electric field is ignored and each fiber mode is normalized, the property of orthogonality requires that any fiber modes m and n be[25]

$$\iint \mathbf{E}^m \cdot \mathbf{E}^{n^*}\mathrm{d}A = \delta_{mn}. \quad (16)$$

From Eqs. (14) and (16) we have

$$\sum_i |a_i|^2 + \sum_v |b_v|^2 = 1, \quad (17)$$

and Eq. (15) can be reduced to

$${\eta_v}^{s-\mathrm{cl}} = \left|\iint \mathbf{E}^s \cdot {\mathbf{E}_v}^{\mathrm{cl}^*}\mathrm{d}A\right|^2 = |b_v|^2. \quad (18a)$$

Similarly, the coupling efficiency between the transformed Gaussian beam and the ith core mode can be expressed as

$${\eta_i}^{s-\mathrm{co}} = \left|\iint \mathbf{E}^s \cdot {\mathbf{E}_i}^{\mathrm{co}^*}\mathrm{d}A\right|^2 = |a_i|^2. \quad (18b)$$

According to coupled-mode theory, only the cladding modes that satisfy both phase matching and strong coupling conditions can be efficiently coupled to the core, whereas the others cannot[26]; i.e.,

$$\lambda_i = \lambda_v \cong \frac{(n^{\mathrm{co}} - {n_v}^{\mathrm{cl}})\Lambda}{\left(1 - \frac{{\kappa_{01-01}}^{\mathrm{co-co}}\Lambda}{2\pi}\right)}, \quad (19)$$

$$\left[({\kappa_{v-01}}^{\mathrm{cl-co}})^2 + \left(\delta + \frac{{\kappa_{01-01}}^{\mathrm{co-co}}}{2}\right)^2\right]^{1/2} L \cong \frac{\pi}{2}, \quad (20)$$

where λ_v denotes the vth resonant wavelength. λ_i is the incident wavelength of the Gaussian beam, n^{co} and ${n_v}^{\mathrm{cl}}$ are the effective indices of the core mode and the vth cladding mode; Λ and L are the period and the length of the LPFG; and ${\kappa_{01\text{-}01}}^{\mathrm{co\text{-}co}}$ and ${\kappa_{v-01}}^{\mathrm{cl\text{-}co}}$ are the coupling coefficients between core-to-core and core-to-vth cladding modes, respectively.

The total coupling efficiency η_{total} is defined as the

power received inside the core in plane Z_4 divided by the total incident power in plane Z_1. For a broadband incident beam, η_{total} can be expressed as

$$\eta_{\text{total}} = \frac{\int P_i \left\{ \left(\sum_v (1 - S_{v,i}) \right) \eta_i^{s-\text{co}} + \sum_v S_{v,i} \eta_{v,i}^{s-\text{cl}} \right\} d\lambda_i}{\int P_i d\lambda_i}, \tag{21}$$

where $S_{v,i}$ is the transmission loss of the vth cladding mode at wavelength λ_i, which can be solved by use of the coupled-mode theory[23]; $\eta_i^{s-\text{co}}$ and $\eta_{v,i}^{s-\text{cl}}$ are the coupling efficiency between the transformed Gaussian beam and the fiber core and the vth cladding modes, respectively, at wavelength λ_i, and P_i is the optical power density carried by λ_i.

If the Gaussian beam is monochromatic and is set to match a specific transmission wavelength of a LPFG, Eq. (21) is simplified to

$$\eta_{\text{total}} = (1 - S_v)\eta^{s-\text{co}} + S_v \eta_v^{s-\text{cl}}. \tag{22}$$

Accordingly, we can solve the total coupling efficiency by using Eqs. (12), (18), and (22). Note that our modeling is based on the following assumptions: that (i) a paraxial approximation is made, (ii) the core region in D_f is not considered, (iii) the longitudinal electric field is not included, and (iv) backreflection scattering is neglected. To estimate the accuracy of the modeling, the energy conservation is calculated in the reference plane Z_3 at various working distances as detailed in Appendix A. The result shows that more than 90% efficiency can be achieved for the working distance within 350 μm.

3. Experiment

Two proofs of experiment are performed to demonstrate the validity of the proposed scheme. In the first experiment, two SMF's of the dispersion-shifted (DS) type are used. The experimental setup is similar to that shown in Fig. 1. SMF1 consists of a LPFG and a lens tip; the output of SMF2 serves as a light source. The far field of SMF2's output has a measured Gaussian fit of ~93.4%. After propagating a working distance Z_s, the Gaussian beam is transformed by a hemispherical lensed fiber with a radius R_f. Depending on the radius of the lens, some cladding modes are excited and then coupled into core mode in region III with the aid of a LPFG. The coupling efficiency can be expressed as $P_{\text{SMF1}}/P_{\text{SMF2}}$, where P_{SMF1} and P_{SMF2} are the received and emitted optical power measured from the output ports of SMF1 and SMF2, respectively.

A wavelength-tunable LD is connected to the input port of SMF2. The wavelength of the LD is chosen to match that of a LPFG that has minimum transmission. The wavelength of the LD has a bandwidth of 0.2 nm at FWHM. A LPFG is imprinted in SMF1 by 248-nm UV exposure through an amplitude mask of period 450 μm. SMF1 was previously hydrogenated for 15 days at a pressure of 1500 psi (~77,570 Torr). The UV exposure area is ~20 mm in length. Because the electric field profile of the HE_{11} mode is similar to the Gaussian form, a higher coupling efficiency can be obtained if the imprinted LPFG is properly designed for the HE_{11} mode. Therefore we need to control the UV-exposure time to obtain the maximum transmission loss for the HE_{11} cladding mode. The evolution of transmission spectrum of the LPFG is monitored *in situ*; it is shown in Fig. 2 for three UV exposure times. Note that the UV-exposure time in the middle spectrum of Fig. 2 is a better choice for the desired LPFG. Moreover, note that the transmission spectrum of the DS fiber shows a strong resonant peak at the first cladding mode. The spectrum is different from the step-index spectrum but similar to those reported previously[27,28] for which two different types of DS fiber were used for LPFG fabrication. The LPFG thus imprinted is then subject to annealing to stabilize its spectral characteristics. SMF1 is cleaved by an electric-arc discharge near the end face of the UV-exposed area to form a hemispherical lens. The radius of curvature can be controlled within a precision of 10 μm. One puts the two SMF's onto the holders of an automatic alignment setup to search for the maximum coupling power in space at a given working distance.

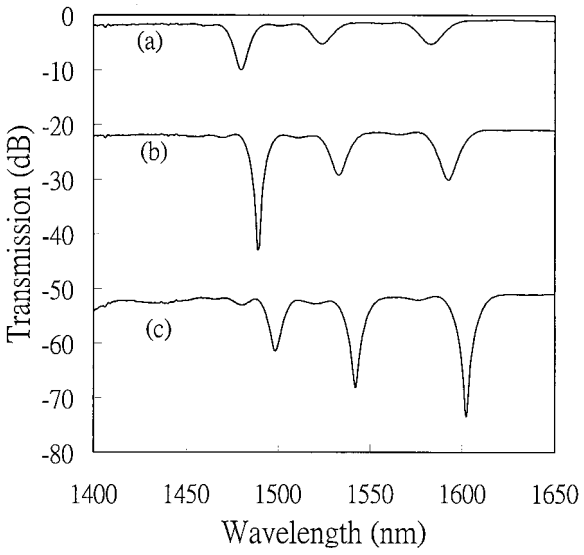

Fig. 2. Evolution of transmission spectra of a LPFG at exposure times (a) 120 s, (b) 180 s, and (c) 210 s.

Figure 3 depicts the variation of coupling efficiency as a function of working distance for a lensed fiber with (solid curve) and without (dashed curve) the LPFG. The corresponding lens radii are 100 and 120 μm. For a lensed fiber without a LPFG, the coupling efficiency reaches the maximum at a short working distance and then decreases monotonically with the separation. The behavior is similar to butt coupling because of the relatively large radii employed. Conversely, for a lensed fiber with a LPFG, the working distance can be relaxed markedly, with a trade-off in efficiency. For a lens radius of 120 μm,

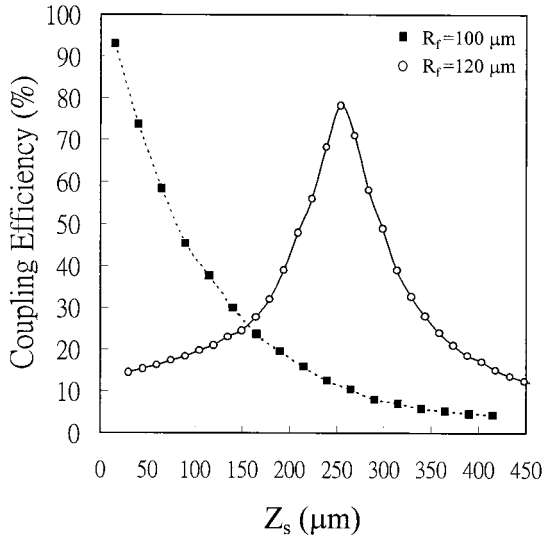

Fig. 3. Coupling efficiency versus working distance for a lensed fiber with (solid curve) and without (dashed curve) the LPFG.

the maximum coupling efficiency is ~78% at a working distance of 250 μm, and the corresponding longitudinal tolerance is ~45 μm at 1-dB loss. For radii of 100, 135, and 180 μm, the optimal working distances are 215, 300, and 375 μm with reduced coupling efficiencies of 58%, 51%, and 43% and their longitudinal tolerances at 1 dB loss are ~50, 60, and 90 μm, respectively. Detailed variation profiles of coupling efficiency as a function of working distance can be found in our earlier paper.[15] Note that, over such a long range of working distance, only a lensed fiber that contains a LPFG can have a high coupling efficiency. For example, over a working distance of ~210 to ~300 μm the coupling efficiency for the fiber with a 120-μm-radius lens is more than 50% and is

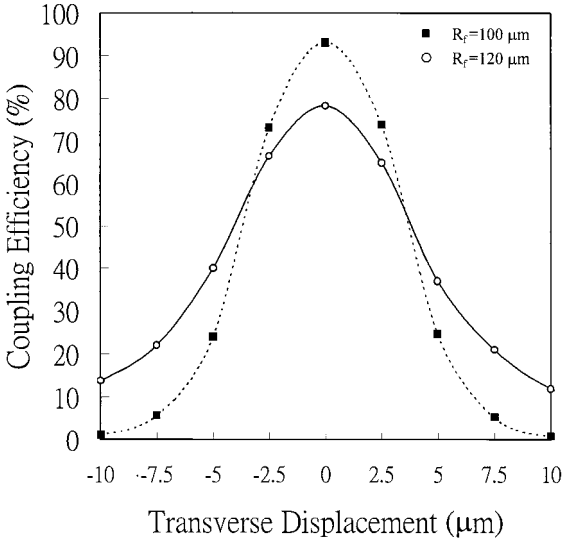

Fig. 4. Coupling efficiency versus transverse displacement for a lensed fiber with (solid curve) and without (dashed curve) the LPFG.

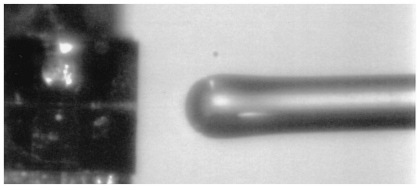

Fig. 5. Microphotograph showing optical coupling between a Fabry–Perot LD and a LPFG lensed fiber.

approximately three to seven times greater than that without the assistance of a LPFG.

Figure 4 shows the variation of coupling efficiency with transverse displacement for a lensed fiber with (solid curve) and without (dashed curve) the LPFG. The corresponding transverse tolerances at 1 dB loss are ~7.6 and ~5 μm, respectively. The other measured transverse tolerances are estimated to be 6.4, 9, and 9 μm for the LPFG fibers with radii of 100, 135, and 180 μm, respectively. All these tolerances are greater than those obtained without the aid of the LPFG.

In the second proof of experiment, a Fabry–Perot-type laser diode operating at a wavelength of 1.56 μm is used as a light source and replaces SMF2. Its far-field profile is measured in parallel and vertical directions with a beam profiler. The measured beam diameters, defined at $1/e^2$ of the maximum intensity, are 658 and 263 μm for the vertical and parallel directions, respectively. As the distance between the end face of LD chip and the sensor head is 470 μm, the near-field beam waists are estimated to be 0.71 and 1.78 μm in the vertical and parallel directions, respectively. The spectral characteristics of the LPFG are adjusted to match the mean wavelength of the LD. Figure 5 is a microphotograph of the optical coupling between a Fabry–Perot LD and a lensed fiber integrated with a LPFG. The lens radius is 70 μm. The transmission of the LPFG and

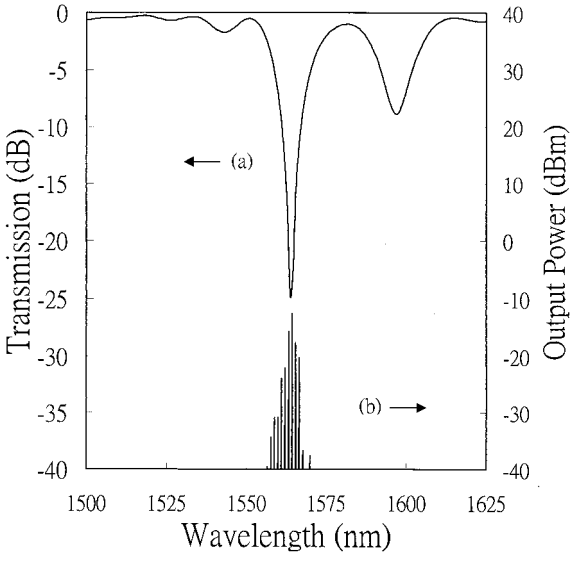

Fig. 6. Spectra of (a) a LPFG and (b) a Fabry–Perot LD.

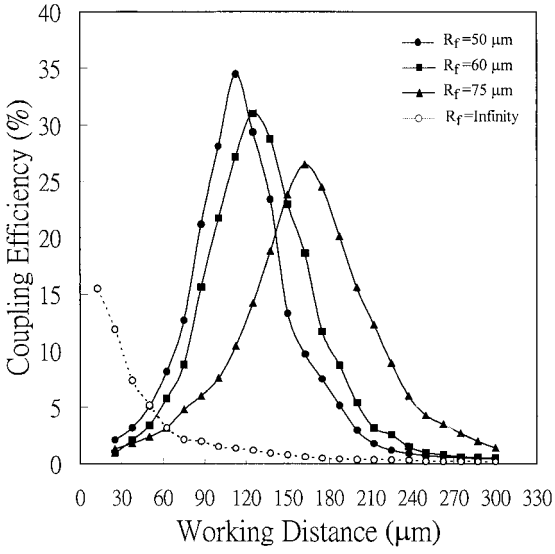

Fig. 7. Measured coupling efficiency versus working distance for lensed fibers with various radii R_f.

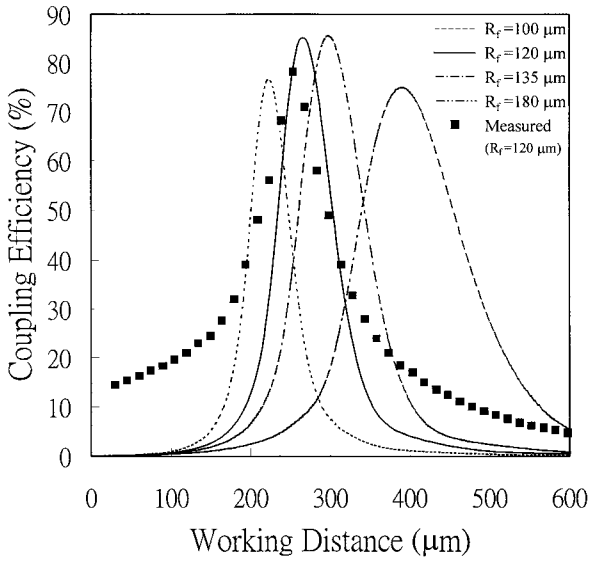

Fig. 8. Simulated coupling efficiency versus working distance for a lensed fiber with various radii R_f. Also shown is the measured result for R_f = 120 μm.

the output spectrum of the Fabry–Perot LD are shown in Fig. 6. The measured 3-dB bandwidth of the LPFG is ~15 nm, larger than the ~1 nm of the LD.

Figure 7 depicts coupling efficiency versus working distance for several radii. The dashed and solid curves correspond to cases of butt coupling (i.e., infinite R_f and without LPFG) and the lensed fiber integrated with a LPFG, respectively. In the case of butt coupling, the maximum coupling efficiency is ~15.5% at a working distance of ~12 μm and then decreases monotonically with separation. Conversely, for a lensed fiber integrated with a LPGF, at such a short working distance only ~1.5% coupling efficiency is measured; however, the efficiency increases to its maximum at a markedly long working distance. For example, for a lens radius of 50 μm, the maximum coupling efficiency is ~34.5% at a working distance of 110 μm, and the corresponding longitudinal tolerance is ~26 μm at 1-dB loss. For other radii, of 60 and 75 μm, the optimal working distances are 125 and 160 μm with corresponding coupling efficiencies of 31% and 26%, respectively. Their longitudinal tolerances at 1-dB loss are ~40 and ~50 μm, respectively. Note that, over such a long range of working distance, only the lensed fiber with LPFG could have a high coupling efficiency. For example, over a working distance of ~85 to ~140 μm the LPFG with a 50-μm-radius lens can have ~10 to ~20 times greater coupling efficiency than that of butt coupling. The transverse tolerances at 1-dB loss of their peak efficiencies are measured as 2.6, 2.8, and 3.2 μm for fibers with radii of 50, 60, and 75 μm, respectively. For comparison, the measured butt-coupling tolerances are ~10 and ~2 μm for longitudinal and transverse directions, respectively, at 1-dB loss.

4. Discussion

In this section we first compare the measured results with the simulated results based on the theory described in Section 2. Then, based on further approximations, we derive the optimal working distance and lens radius. Moreover, we discuss some important considerations when the proposed new scheme is practically applied.

A. Simulation Results

The radial and azimuthal electric field of a fiber cladding mode can be obtained by solution of the problem of a three-layer, step-index, weakly guiding SMF subjected to the boundary conditions at each interface.[23] The following parameters are assumed: index of core, n_{co} = 1.458; index of cladding, n_{cl} = 1.45; radius of core, a_{co} = 2.75 μm; radius of cladding, a_{cl} = 62.5 μm; and mode field diameter of incident Gaussian beam, W_0 = 6.5 μm. Thus the total coupling efficiency as a function of working distance can be solved numerically with Eqs. (12), (18), and (22). Figure 8 shows the simulation results for various radii of lensed fibers in an ideal case; i.e., when the transmission of HE_{11} of the LPFG is zero. Here we ignore the thickness D_f of the lensed fiber. The calculated maximum coupling efficiencies are found to be approximately 76%, 86%, 85%, and 75% for R_f of 100, 120, 135, and 180 μm, respectively. The estimated corresponding longitudinal tolerances at 1 dB are approximately 35, 45, 55, and 85 μm, which are similar to the measured tolerances. However, there are some discrepancies between the simulated and measured results. First, all simulated results show narrower tolerances, especially at the tail ends. Second, the calculated maximum coupling efficiencies differ from the measured ones. These results can be attributed to the following situations: (1) The

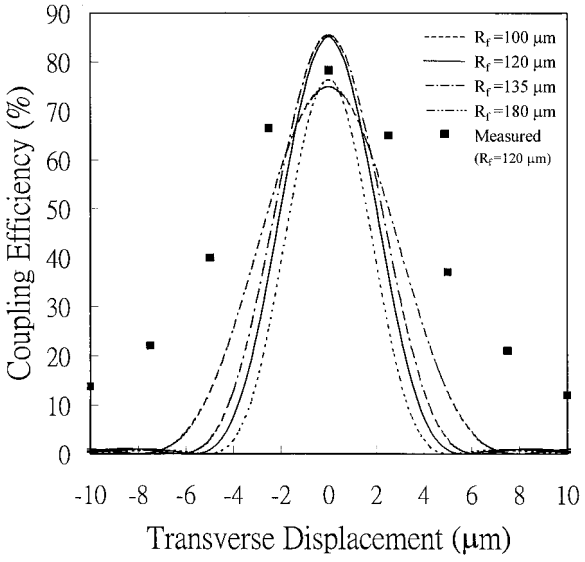

Fig. 9. Simulated coupling efficiency versus transverse displacement for a lensed fiber with various radii R_f. Also shown is the measured result for R_f = 120 μm.

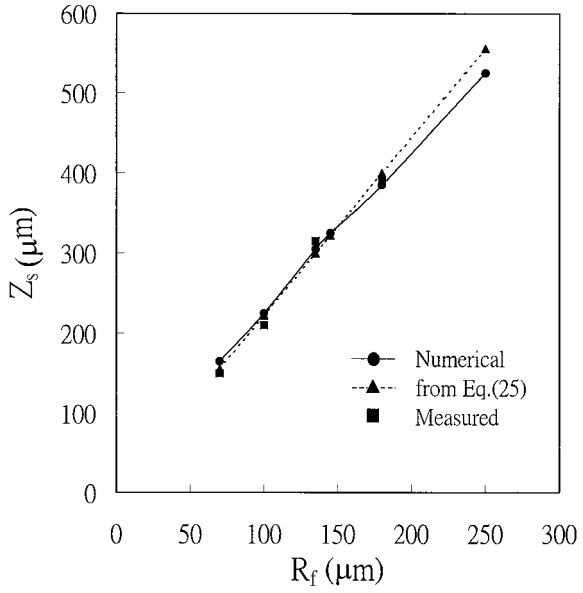

Fig. 10. Variation of optimal working distance with radii of a lensed fiber.

index profile of the DS fiber used in the experiment has a shape that is closer to that of a triangle than to a step shape as used in the simulation; therefore the actual electrical field distribution is different from the simulated one. (2) The bending is induced during the assembly of the LPFG; therefore the transmission loss of the LPFG will be strongly reduced and the resonant peak will be shifted to the longer-wavelength side. (3) We ignore the existence of the core in region II of our model and find that the transformed Gaussian beam may be slightly distorted. The reason for our not using a common step-index fiber for the experiment is that the transmission of the HE_{11} mode thus fabricated is relatively weak, only −1 to −2 dB for a strong LPFG.[23] Moreover, we observe that the HE_{11} mode of a LPFG made from a DS fiber is almost insensitive to the surrounding medium, a property that makes further recoating of the fiber easier.

Figure 9 shows simulated coupling efficiency versus transverse displacement for lensed fibers with various radii. The simulated transverse tolerances at 3-dB loss for R_f = 100, 120, 135, 180 μm are approximately 4, 4.5, 5, and 6.5 μm, respectively. The measured transverse tolerance is larger than the simulated tolerance for the same reasons as described above.

B. Optimal Working Distance

An approximate working distance of the vth cladding mode for the maximum coupling efficiency, defined as $Z_{s,\mathrm{optm}}{}^{v}$, can be derived if the radius of the lensed fiber is given. Using Eqs. (6), (7), (10), and (11) and assuming that $D_f = d_x = 0$, we have

$$R_{x3} = \frac{n_{\mathrm{cl}} R_f R_2}{n_1 R_f - R_2(n_{\mathrm{cl}} - n_1)},$$

$$W_{x3} = W_{x2}. \tag{23}$$

Based on the ray optics approximation, the guided angle for the vth cladding mode can be estimated as $\theta_v{}^{\mathrm{cl}} = (\pi/2) - \theta_3 = \cos^{-1}(n_{1v}{}^{\mathrm{cl}}/n_{\mathrm{cl}})$, where $n_{1v}{}^{\mathrm{cl}}$ denotes the effective index of the vth cladding mode. To obtain an analytical solution for the optimal working distance we assume that $\theta_v{}^{\mathrm{cl}} \sim \pm W_{x3}/R_{x3}$, where + and − correspond to divergent and convergent wave fronts, respectively. By using Eqs. (2), (3), and (23) as well as assuming that $Z_s/Z_0 \gg 1$, we can approximate the optimal working distance for the vth cladding mode as

$$Z_{s,\mathrm{optm}}{}^{v} \approx \left(\frac{R_f}{n_{\mathrm{cl}} - n_1}\right)\left[n_1 \pm \frac{\pi W_0 n_{\mathrm{cl}} \theta_v{}^{\mathrm{cl}}}{\lambda_i}\right], \tag{24}$$

$$Z_{s,\mathrm{optm}}{}^{1} \approx \frac{n_1 R_f}{n_{\mathrm{cl}} - n_1}. \tag{25}$$

Expression (25) is obtained for the HE_{11} mode because the magnitude of $\theta_1{}^{\mathrm{cl}}$ is very small ($\sim \pm 0.00872$ rad for λ_i = 1.51 μm). Therefore the working distance for the maximum coupling efficiency increases linearly with the lens radius, as shown in Fig. 10, in which the approximate result is seen to be similar to those from numerical and measured calculations. The optimal working distance of the HE_{11} mode is located near the focal plane of the hemispherical lens, implying that the wave front that is characteristic of a HE_{11} mode is approximately a plane wave.

C. Optimal Lens Radius

It is important to find the optimal radius of a lensed fiber for the maximum coupling efficiency when the LPFG parameters, wavelength, and mode field diameter of the incident Gaussian beam are given. Unfortunately, there is no analytical solution. For

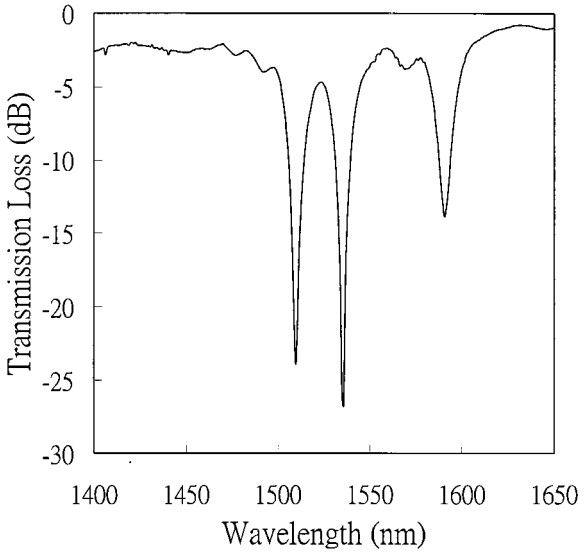

Fig. 11. Transmission spectrum of the LPFG used for coupling of the HE_{11} and HE_{13} modes.

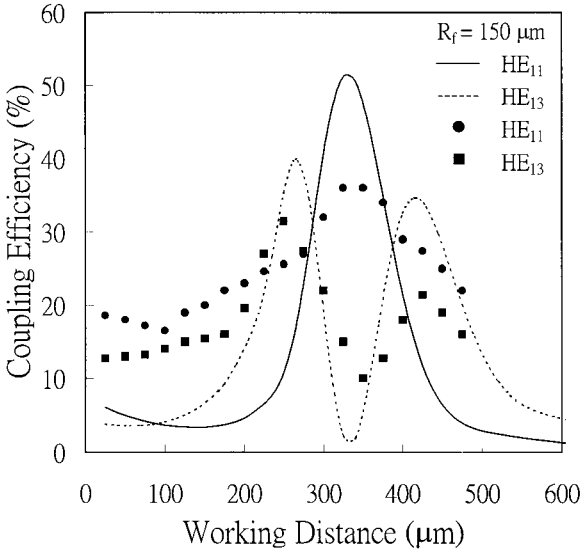

Fig. 12. Measured and simulated coupling efficiencies of HE_{11} and HE_{13} modes versus working distance.

estimation, we assume only that the transformed Gaussian beam that satisfies the following condition can lead to the maximum coupling for the HE_{11} mode:

$$W_{3,\mathrm{optm}} = C r_{\max}^{\mathrm{cl}}, \tag{26}$$

where $W_{3,\mathrm{optm}}$ is the waist of the transformed Gaussian beam at the optimal working distance $Z_{s,\mathrm{optm}}{}^{1}$ for the optimal lens radius; $r_{\max}{}^{\mathrm{cl}}$ is the radial position of the maximum magnitude of the HE_{11} cladding mode obtained by definition of a three-layer step-index SMF, and C is an adjustable parameter. Therefore, from Eqs. (2) and (23) and expression (25), the optimal radius $R_{f,\mathrm{optm}}{}^{11}$ can be expressed as

$$R_{f,\mathrm{optm}}{}^{11} = \frac{C\pi W_0 r_{\max}{}^{\mathrm{cl}}(n_{\mathrm{cl}} - n_1)}{n_1 \lambda_1}, \tag{27}$$

where W_0 and λ_i are the waist and the wavelength, respectively, of the incident Gaussian beam. Using the same parameters and $r_{\max}{}^{\mathrm{cl}} = 26$ μm and assuming that $W_{3,\mathrm{optm}} \approx 1.8 r_{\max}{}^{\mathrm{cl}}$, we have $R_{f,\mathrm{optm}}{}^{11} \sim 140$, 48 μm for SMF-to-SMF and LD-to-SMF coupling, respectively. The results are consistent with the calculated ones, i.e., $R_{f,\mathrm{optm}}{}^{11} \sim 138$, 45 μm, which we obtained by numerically solving Eqs. (12), (18), and (22) for various radii $R_f{}^{11}$.

D. Mode Dependence

To distinguish the coupling efficiencies that resulted from HE_{11} and HE_{13} modes we use a fiber with a radius of curvature of ~145 μm and the transmission spectrum in Fig. 11. For measurement of coupling efficiencies, the laser diode is tuned to match the resonant wavelengths of the LPFG, i.e., $\lambda_i = 1510$ nm and $\lambda_i = 1536$ nm for HE_{11} and HE_{13}, respectively. The experimental relationship of coupling efficiency to working distance is shown in Fig. 12. Note there are two maxima of working distances (250 and 425 μm) for the HE_{13} mode but only one maximum (~325 μm) for the HE_{11} mode. The coupling efficiency shows a linear decay only for the HE_{11} mode but not for the HE_{13} mode at small working distances, perhaps because of a relatively weak loss for the HE_{11} mode. Therefore a portion of beam is directly coupled into the core and remains propagating in the core at shorter working distances.

Also shown in Fig. 12 is the relationship of simulated coupling efficiency to working distance for the HE_{11} and HE_{13} cladding modes. The parameters remain the same, except that losses S are assumed to be 0.65 and 0.8 for modes HE_{11} and HE_{13}, respectively. There are two local maxima of coupling efficiency for the HE_{13} mode. Note that the location of the maximum coupling efficiency of the HE_{11} mode is exactly the same as that of the local minimum of the HE_{13} mode, which can be understood from the law of energy conservation even though the resonant HE_{11} and HE_{13} wavelengths are slightly different. Because most of the energy of the incident Gaussian beam is transformed into mode HE_{11} at plane Z_3 at the optimal working distance $Z_{s,\mathrm{optm}}{}^{1}$, no other cladding modes will be excited. The simulated longitudinal and transverse tolerances at 1-dB loss are estimated to be approximately 20–25 and 1.5–1.8 μm, respectively, for HE_{13} coupling. The location of the maximum coupling efficiency for HE_{13} can be estimated from expression (24). The calculated effective index $n_{13}{}^{\mathrm{cl}}$ of the HE_{13} mode is 1.4497 for $\lambda_i = 1.53$ μm, which we obtain by modeling the fiber as a three-layer step-index structure, and its corresponding guided angle is 1.048°. Therefore the locations of maximum coupling efficiency are ~280 and ~390 μm. However, as shown in Fig. 12, the corresponding measured locations are ~265 and ~415 μm. The difference is relatively larger than for the HE_{11} mode because the guided angle of HE_{13} is twice as long as that of HE_{11}. Although the approximate re-

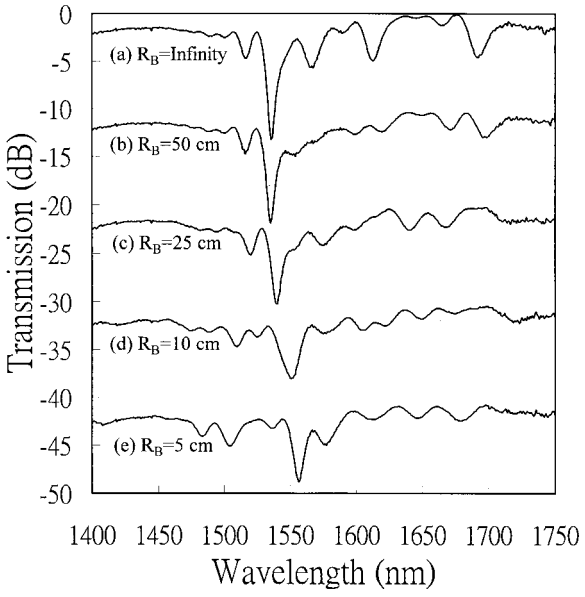

Fig. 13. Evolution of transmission spectra at various bend radii R_B.

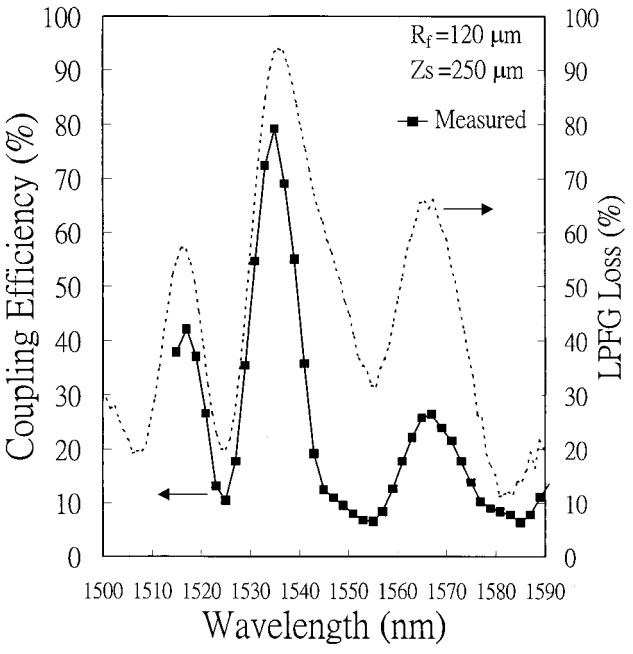

Fig. 14. Measured dependence of coupling efficiency and loss of LPFG (dashed curve) on wavelength.

sult is slightly different from the simulated one, it still provides a good first-order estimation.

E. Bending Effect

Because the transmission spectrum of a LPFG is highly sensitive to external bending, the resonant peak of the LPFG will shift to the longer-wavelength side and the transmission loss will change drastically. Figure 13 shows the experiment results for various bending radii R_B. Therefore it is important to avoid excess bending on a LPFG in the practical packaging process when such a scheme is applied for optical coupling.

F. Wavelength and Temperature Dependence

Inasmuch as only the modes that satisfy the phase-matching condition can be efficiently coupled into the core, the proposed coupling scheme is obviously wavelength dependent. Figure 14 depicts the dependence of coupling efficiency on wavelength at the optimal working distance, i.e., Z_s = 250 μm, and the loss spectrum of the integrated LPFG. It can be seen that the coupling efficiency almost follows the loss spectrum of the LPFG, which can be understood from Eq. (22) because the coupling efficiency η_{total} is almost proportional to the LPFG loss S_v if $\eta_v^{s-\text{cl}}$ is larger than $\eta^{s-\text{co}}$. The ratio of $\eta_1^{s-\text{cl}}$ at the maximum peak, i.e., λ = 1535 nm, is estimated to be 84%, which is close to the theoretical value of 88%. In general, a LPFG is temperature sensitive; thus the phase-matching condition may change with the environment, resulting in variations of coupling efficiency. The problem can be solved, for example, by use of a novel temperature-insensitive long-period fiber grating.[29]

5. Conclusions

A lensed fiber is considered more stable and compact than a nonlensed fiber in optical coupling. However, in most cases it is practically difficult to assemble and mass produce a lensed fiber owing to its small working distance and critical lens radius. Here we propose a novel optical coupling scheme that uses a hemispherical lensed fiber integrated with a LPFG. The proposed novel coupling scheme was demonstrated in both SMF-to-SMF and LD-to-SMF proofs of experiment. A coupling efficiency of ~78% was obtained with a lens radius of ~120 μm at a working distance of ~250 μm when the wavelength of the incident Gaussian beam was tuned to match the resonant wavelength of the HE_{11} cladding mode. As for HE_{13} coupling, two working distances that lead to the maxima of coupling efficiency were found.

We employed a model based on an *ABCD* matrix and mode expansion to calculate the coupling efficiency at various working distances. The results show that (1) utilization of the novel coupling scheme results in a long working distance because most of the launched beam is coupled to the cladding rather to the core, (2) maximum efficiency can be obtained in HE_{11} coupling because of the similar Gaussian profile but not in other cladding modes, and (3) the calculated working distance and the longitudinal tolerance for the maximum coupling efficiency are consistent with measured ones for both HE_{11} and HE_{13} coupling.

Based on a ray optics approximation, an optimal working distance and an optimal lens radius were derived for the maximum coupling efficiency. These approximate results are in good agreement with the calculated and measured ones. Achieving the max-

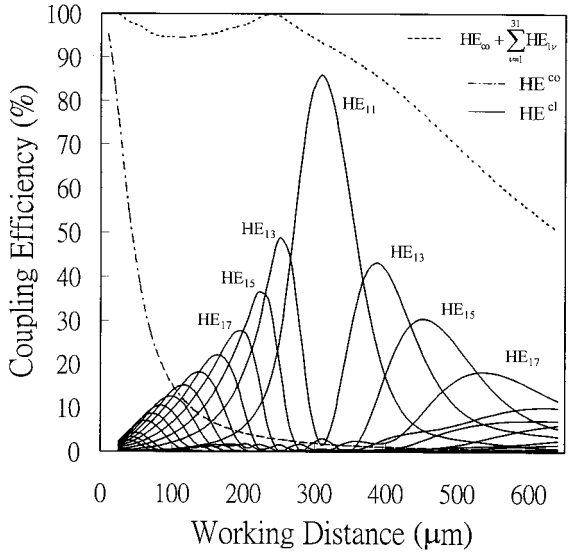

Fig. 15. Simulated coupling efficiencies and their sum versus working distance for various cladding and core modes.

imum coupling efficiency requires that the following conditions be fulfilled: (i) HE_{11} coupling is preferred, (ii) the lens radius should be matched to Eq. (27), (iii) the Gaussian beam waist should be positioned as directed by expression (25), (iv) the wavelength between the incident Gaussian beam and the resonant peak of the HE_{11} mode should be matched, (v) the transmission loss for the HE_{11} mode should be as strong as possible, and (vi) external bending and a wavelength-shift effect should be avoided in the practical application.

Appendix A

In Section 2 we assume that the transformed Gaussian beam can be expanded by use of a complete set derived from a three-layer fiber mode. As shown by Eqs. (14)–(18), the total coupling efficiency η_{total}, defined as $\eta_{\text{total}} = \sum_{v=1}^{v=\infty} \eta^{s-\text{co}} + \eta_v^{s-\text{cl}}$, should be equal to unity for any working distance from the viewpoint of energy conservation. To estimate the accuracy of our model, we discuss the energy conservation at reference plane Z_3 for various working distances. The radius of curvature is chosen to be 140 μm because there the simulated coupling efficiency becomes maximum, as mentioned in Subsection 4.C. Other parameters are the same as described in Section 4, except that $D_f = 0$ and $S = 0, 1$ for the core and the cladding modes, respectively. Figure 15 shows the simulated coupling efficiency versus working distance for various even cladding modes and a core mode. The odd cladding modes are not shown because of their relatively weak magnitudes. The total coupling efficiency η_{total} is obtained from the first 16 even cladding modes. That the total coupling efficiency is more than 90% as the working distance is 350 μm or less but decreases almost linearly as the working distance increases. The waist of Gaussian beam is ~56 μm in plane Z_3 for $Z_s = 350$ μm and becomes ~96 μm for $Z_s = 600$ μm. As the working distance becomes greater than 350 μm, the beam size exceeds the fiber's diameter and causes the total coupling efficiency to decrease; a portion of the Gaussian beam could become radiation modes and escape from the cladding–air interface. Note that there is still a discrepancy between the simulated result and the ideal one, i.e., $\eta_{\text{total}} = 1$, possibly because of the finite superposition of the cladding modes.

The authors thank S. H. Tseng and G. W. Chern for their assistance in the calculation of the three-layer fiber mode, C. D. Su for helpful discussions, and the Industrial Technology Research Institute/Opto-Electronics and System Laboratories for providing the beam profiler. The authors are grateful for partial support by the National Science Council, Taiwan, under contract NSC 89-2215-E-002-013 and by the Education Ministry of Taiwan under contract 89-E-FA06-2-4.

References

1. A. M. Vengsakar, P. J. Lemaire, J. B. Judkins, V. Bhatia, T. Erdogan, and J. Sipe, "Long-period fiber gratings as band-rejection filters," J. Lightwave Technol. **4,** 58–65 (1996).
2. A. M. Vengsakar, J. R. Pedrazzani, J. B. Judkins, and P. J. Lemaire, "Long-period fiber-grating-based gain equalizers," Opt. Lett. **21,** 336–338 (1996).
3. D. C. Johnson, F. Bilodeau, B. Malo, K. O. Hill, P. G. J. Wigley, and G. I. Stegeman, "Long-length, long-period rocking filters fabricated from conventional monomode telecommunications optical fiber," Opt. Lett. **17,** 1635–1637 (1992).
4. K. O. Hill, B. Malo, K. A. Vineberg, F. Bilodeau, D. C. Johnson, and I. Skinner, "Efficient mode conversion in telecommunication fiber using externally written gratings," Electron. Lett. **26,** 1270–1272 (1990).
5. V. Bhatia and A. M. Vengsarkar, "Optical fiber long-period grating sensors," Opt. Lett. **21,** 692–694 (1996).
6. J. Yamada, Y. Murakami, J. Sakai, and T. Kimura, "Characteristics of a hemispherical microlens for coupling between a semiconductor laser and single-mode fiber," IEEE J. Quantum. Electron. **QE-16,** 1067–1072 (1980).
7. H. Kuwahara, M. Sasaki, and N. Tokoyo, "Efficient coupling from semiconductor lasers into single-mode fibers with tapered hemispherical ends," J. Lightwave Technol. **14,** 58–65 (1996).
8. C. Edwards, H. Presby, and C. Dragone, "Ideal microlenses for laser to fiber coupling," J. Lightwave Technol. **11,** 252–257 (1993).
9. W. L. Emkey and C. A. Jack, "Analysis and evaluation of graded-index fiber-lenses," J. Lightwave Technol. **5,** 1156–1164 (1987).
10. K. Shiraishi, "A lensed fiber with a long working distance for integrated coupling between laser diodes and single-mode fibers," J. Lightwave Technol. **13,** 1736–1744 (1995).
11. W. Bludau and R. H. Rosserg, "Low-loss laser-to-fiber coupling with negligible optical feedback," J. Lightwave Technol. **LT-3,** 294–302 (1985).
12. I. Moerman, P. P. Van Daele, and P. M. Demeester, "A review on fabrication technologies for the monolithic integration of tapers with III–V semiconductor devices," IEEE J. Sel. Top. Quantum. Electron. **3,** 1308–1320 (1997).
13. N. Kalonji and J. Semo, "High efficiency long working distance laser diode to singlemode fiber coupling arrangement," Electron. Lett. **30,** 892–893 (1994).
14. P. Chanclou, M. Thual, J. Lostec, P. Auvray, J. Caulet, G. Joulié, A. Poudoulec, and B. Clavel, "Highly efficient collective

coupling between laser diode array and lensed fiber ribbon," Electron. Lett. **34,** 273–274 (1998).
15. W. T. Chen and L. A. Wang, "Optical coupling between singlemode fibers by utilizing long-period fibre grating," Electron. Lett. **35,** 421–423 (1999).
16. H. J. Patrick, C. G. Askins, R. W. McElhanon, and E. J. Friebel, "Amplitude mask patterned on an excimer laser mirror for high intensity writing of long period fiber gratings," Electron. Lett. **33,** 1167–1168 (1997).
17. E. M. Dianove, D. S. Stardubov, S. A. Vasiliev, A. A. Frolov, and O. I. Medvedkov, "Refractive-index gratings written by near-ultraviolet radiation," Opt. Lett. **22,** 221–223 (1997).
18. D. D. Davis, T. K. Gaylord, E. N. Glytsis, and S. C. Mettle, "CO_2 laser-induced long-period fiber gratings: spectral characteristics, cladding modes and polarisation independence," Electron. Lett. **34,** 1416–1417 (1998).
19. T. Enomoto, M. Shigehara, S. Ishikawa, T. Danzuka, and H. Kanamori, "Long-period fiber grating in a pure-silica-core fiber written by residual stress relaxation," in *Optical Fiber Communication Conference* (*OFC*), Vol. 2 of 1998 OSA Technical Digest Series (Optical Society of America, Washington, D.C., 1998), paper ThG2.
20. H. Kogelnik, "On the propagation of Gaussian beams of light through lenslike media including those with a loss or gain variation," Appl. Opt. **4,** 1562–1569 (1965).
21. G. A. Massey and A. E. Siegman, "Reflection and refraction of a Gaussian light beam at tilted ellipsoidal surfaces," Appl. Opt. **8,** 975–978 (1969).
22. J.-I. Sakai and T. Kimura, "Design of a miniature lens for semiconductor laser to single-mode fiber coupling," IEEE J. Quantum Electron. **QE-16,** 1059–1066 (1980).
23. T. Erdogan, "Cladding-mode resonances in short- and long-period fiber grating filters," J. Opt. Soc. Am. A **14,** 1760–1773 (1997).
24. D. Marcuse, *Theory of Dielectric Optical Waveguides* (Academic, Boston, Mass., 1991), Chaps. 2 and 3.
25. A. Yariv and P. Yeh, *Optical Waves in Crystals* (Wiley, New York, 1983), Chap. 11.
26. T. Erdogan, "Fiber grating spectra," J. Lightwave Technol. **15,** 1277–1294 (1997).
27. H. J. Patrick, A. D. Kersey, and F. Bucholtz, "Analysis of the response of long period fiber grating to external index of refraction," J. Lightwave Technol. **16,** 1606–1611 (1998).
28. B. H. Lee and J. Nishii, "Cladding-surrounding interface insensitive long-period grating," Electron. Lett. **34,** 1129–1130 (1998).
29. K. Shima, K. Himeno, T. Sakai, S. Okude, A. Wada, and R. Yamauchi, "A novel temperature-insensitive long-period fiber grating using a boron-codoped-germanosilicate-core fiber," in *Optical Fiber Communication Conference*, Vol. 6 of 1997 OSA Technical Digest Series (Optical Society of America, Washington, D.C., 1997), paper FB2.